Journal of Power Sources 196 (2011) 6924–6928

Contents lists available at ScienceDirect

Journal of Power Sources

journal homepage: www.elsevier.com/locate/jpowsour

Short communication

Enhanced electrochemical performance of carbon–$LiMn_{1-x}Fe_xPO_4$ nanocomposite cathode for lithium-ion batteries

Seung-Min Oh[a,b], Hun-Gi Jung[a], Chong Seung Yoon[c], Seung-Taek Myung[d], Zonghai Chen[e], Khalil Amine[e,*], Yang-Kook Sun[a,b,**]

[a] Department of WCU Energy Engineering, Hanyang University, Seoul 133-791, South Korea
[b] Department of Chemical Engineering, Hanyang University, Seoul 133-791, South Korea
[c] Department of Materials Science and Engineering, Hanyang University, Seoul 133-791, South Korea
[d] Department of Chemical Engineering, Iwate University, 4-3-5 Ueda, Morioka, Iwate 020-8551, Japan
[e] Electrochemical Technology Program, Chemical Sciences and Engineering Division, Argonne National Laboratory, 9700 South Cass Avenue, Argonne, IL 60439, USA

ARTICLE INFO

Article history:
Received 1 October 2010
Received in revised form
23 November 2010
Accepted 24 November 2010
Available online 7 December 2010

Keywords:
Carbon coating
Olivine
Iron doping
Nanocomposite
Lithium battery

ABSTRACT

4 V-class olivine C–$LiMn_{1-x}Fe_xPO_4$ (x = 0 and 0.15) are synthesized by ultrasonic pyrolysis followed by ball milling with AB carbon to evaluate the doping effect of iron. The C–$LiMn_{0.85}Fe_{0.15}PO_4$ shows excellent rate capability having discharge capacity of 150 mAh g^{-1} at 0.5C-rate and 121 mAh g^{-1} at 2C-rate. The capacity retention of the C-$LiMn_{0.85}Fe_{0.15}PO_4$ is 91% after 50 cycles at 55 °C whereas C–$LiMnPO_4$ is limited to 87%. The improved electrochemical performance of the C–$LiMn_{0.85}Fe_{0.15}PO_4$ electrode is attributed to the enhanced electrical conductivity caused by tighter binding on the carbon particles with the $LiMn_{0.85}Fe_{0.15}PO_4$ primary particles as well as by the surface coating of carbon on the primary particles.

Published by Elsevier B.V.

1. Introduction

Recently, olivine-type $LiMPO_4$ (M=Fe, Mn, Co, and Ni) has been extensively studied as promising cathode materials for lithium-ion batteries because the demand for cheap and safer batteries is increased driven by increased market for transportation and energy storage. Among them, $LiFePO_4$ has been regarded as the most promising cathode material due to its low cost, environmental friendly, and thermal stability [1,2]. However, this material has low electrochemical performance caused by poor electronic conductivity [1]. This disadvantage had been successfully overcome by reducing the $LiFePO_4$ particles to a nano-scale [2–7] and coating $LiFePO_4$ particles surface with carbon [8,9], and supervalent cation doping [2]. Isostructural $LiMnPO_4$ could also be very promising cathode active materials due to its higher redox potential (4.1 V vs. Li/Li^+) than that of $LiFePO_4$ (3.4 V vs. Li/Li^+). Due to the strong bonding characteristics of PO_4^{3-}, the $LiMnPO_4$ demonstrated an excellent cycle and thermal stability compared to lithium transition metal oxides of $LiCoO_2$, $LiNi_{0.8}Co_{0.15}Al_{0.05}O_2$, and $LiMn_2O_4$. However, $LiMnPO_4$ also has very poor electronic conductivity (<10^{-10} S cm^{-1}) which is even lower than that of $LiFePO_4$ (1.8×10^{-8} S cm^{-1}), which leads to lower capacity and poor rate capability [10].

Similar to $LiFePO_4$, several approaches have been proposed to improve electrochemical performance of $LiMnPO_4$ by (i) preparing nano-sized $LiMnPO_4$ particles to reduce Li^+ diffusion length [11–21] and (ii) either coating them with nano-layer carbon [11–19] or (iii) doping nano-$LiMnPO_4$ with cations (Mg, Ti, Zr, Fe, and Zn) [20,21] to enhance the electronic conductivity. Various synthetic methods based on above approaches have been applied [11–21]. Among those, the wet synthetic method is more efficient to prepare nano-sized $LiMnPO_4$ powders [13–19]. Delacourt et al. synthesized 100 nm-$LiMnPO_4$ powders by a direct precipitation method, which delivered a discharge capacity of 80 mAh g^{-1} at 1/20C-rate [13]. Drezen et al. reported that 140 nm-$LiMnPO_4$ synthesized by sol–gel method followed by carbon coating demonstrated a reversible capacity of 134 mAh g^{-1} at 1/10C-rate [14]. Recently, 25–30 nm-sized $LiMnPO_4$ particles synthesized by polyol method showed a relatively higher discharge capacity of 140 mAh g^{-1} at 1/10C-rate while improved rate capability compared with previously reported results [16]. More recently, we synthesized an electrically conducting carbon–$LiMnPO_4$ nanocomposite by ultrasonic spray pyrolysis

* Corresponding author. Tel.: +1 630 252 3838; fax: +1 630 972 4451.
** Corresponding author at: Department of WCU Energy Engineering, Hanyang University, Seoul 133-791, South Korea. Tel: +82 2 2220 0524; fax: +82 2 2282 7329.
E-mail addresses: amine@anl.gov (K. Amine), yksun@hanyang.ac.kr (Y.-K. Sun).

0378-7753/$ – see front matter. Published by Elsevier B.V.
doi:10.1016/j.jpowsour.2010.11.159

followed by ball milling with carbon [19]. 30 wt.% carbon–$LiMnPO_4$ nanocomposite delivered a reversible capacity of 155 mAh g^{-1} at 1/10*C*-rate, and exhibited an excellent rate capability and good cycle life. The improved properties were ascribed to the homogeneous coating of the acetylene black (AB) carbon, which protected the C–$LiMnPO_4$ against HF attack, leading to a significant reduction in Mn dissolution, a lower charge-transfer resistance, and a greatly enhanced electronic conductivity. Based on the above reports, we conclude that the combined effect of uniform carbon coating and nanostructuring on $LiMnPO_4$ is crucial parameters to determine electrochemical properties.

It has been reported that $Li[Mn_{1-x}Fe_x]PO_4$ had a higher rate capability and larger reversible capacity than $LiMnPO_4$ with the localization of small polaronic holes on Mn^{2+} sites [1,21–23]. However, it is important to minimize the Fe content in the compound since redox potential of $Fe^{2+/3+}$ is only 3.4 V. In this study, we report the electrochemical performance of a nanostructured C–$LiMn_{1-x}Fe_xPO_4$ (x = 0 and 0.15) (hereafter referred to "C–$LiMn_{1-x}Fe_xPO_4$") prepared by ultrasonic spray pyrolysis followed by ball milling with acetylene black (AB).

2. Experimental

We prepared $LiMn_{1-x}Fe_xPO_4$ (x = 0 and 0.15) powder by an ultrasonic spray pyrolysis method and followed by ball milling with AB carbon. Stoichiometric amounts of lithium dihydrogen phosphate acid (LiH_2PO_4, Sigma) and manganese nitrate tetrahydrate ($Mn(NO_3)_2{\cdot}4H_2O$, Sigma) and iron nitrate nonahydrate ($Fe(NO_3)_3{\cdot}9H_2O$, Sigma) were dissolved in distilled water [molar ratio of Li(PO_4)/Mn/Fe = 1:1:0 and 1:0.85:0.15]. The dissolved solution was added to a citric acid and sucrose aqueous solution (molar ratio of $LiMn_{1-x}Fe_xPO_4$/citric acid/sucrose = 1:0.2:0.05). Atomization of the starting solution was performed with an ultrasonic nebulizer having a resonant frequency of 1.7 MHz. The aerosol stream was introduced into a vertical quartz reactor heated to 400 °C. The inner diameter and length of the quartz reactor were 50 and 1200 mm, respectively. The flow rate of the air used as a carrier gas was 10 L min^{-1}. The obtained powders were then heat treated at 500 °C for 1 h in an air atmosphere (hereafter referred to as "precursor"). The precursor was mixed with 30 wt.% AB carbon. The $LiMn_{1-x}Fe_xPO_4$ and AB carbon mixture was heated at 500 °C for 1 h in an Ar gas flow.

Then synthesized material was characterized by various methods. Powder X-ray diffraction (XRD, Rint-2000, Rigaku, Japan) using Cu-Kα radiation was employed to identify the crystalline phase. Particle morphologies of the precursor and C–$LiMn_{1-x}Fe_xPO_4$ powder were determined by scanning electron microscopy (SEM, JSM 6400, JEOL) and transmission electron microscopy (TEM, JEOL, 2010). The conductivity of disc-shaped pellets for the synthesized material was measured by the four-point DC method at 25 °C. An elemental analyzer (EA110, CE Instrument) was employed to determine the amount of carbon in the final products. To measure the extent of Mn dissolution into the electrolyte, cells charged to 4.5 V were carefully disassembled, and the active materials were stored in electrolyte at 55 °C for 4 weeks. The electrolyte was 1 M $LiPF_6$ in a 1:1 mixture of ethylene carbonate (EC) and diethyl carbonate (DEC). The amounts of dissolved Mn in the electrolyte were measured by atomic absorption spectroscopy (Analytik Jena AG, Vario 6).

Galvanostatic charge/discharge cycling was performed with 2032-type coin cells. The cathodes were fabricated from a mixture of C–$LiMn_{1-x}Fe_xPO_4$ powder (85 wt.%), carbon black (7.5 wt.%), and polyvinylidene fluoride (PVDF) (7.5 wt.%) in N-methyl-2-pyrrolidone. The slurry was then cast on aluminum foil and dried at 110 °C overnight under vacuum. Lithium foil (Cyprus Foote Mineral Co.) was used as the anode. The electrolyte solution used was 1 M $LiPF_6$ in an EC and DEC mixture in a 1:1 volume ratio (PANAX ETEC Co., Korea). The cells were cycled in a constant current-constant voltage mode at a 1/20*C*-rate to 4.5 V, held at 4.5 V until 1/100*C*-rate, and then discharged to 2.7 V at a specific rate (where 1*C* = 170 mAh g^{-1}).

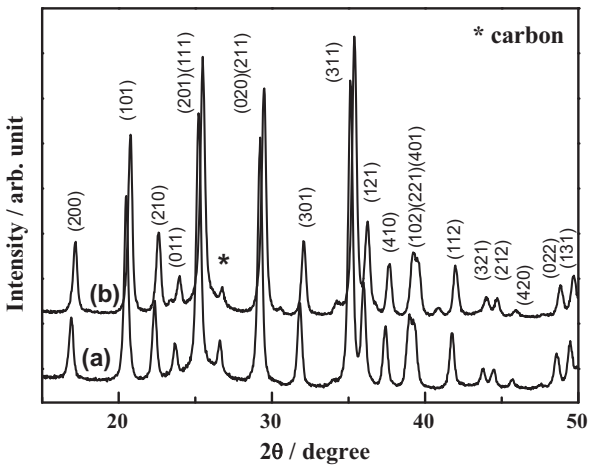

Fig. 1. XRD patterns of C–$LiMn_{1-x}Fe_xPO_4$ powders: (a) x = 0 and (b) x = 0.15.

3. Results and discussion

Fig. 1 shows the XRD patterns of C–$LiMn_{1-x}Fe_xPO_4$ powders (x = 0 and 0.15). The two samples are pure olivine-type $LiMnPO_4$ with *Pnmb* space group. Carbon was detected as impurity phase. The diffraction peaks of C–$LiMn_{0.85}Fe_{0.15}PO_4$ slightly shifted to higher degree due to addition of iron [24]. Lattice parameters calculated by the least square method are represented in Table 1, showing that the unit cell was slightly compressed by the Fe doping. The reduction in the unit cell volume likely stemmed from the difference in the ionic radii since ionic radius of Fe^{2+} (0.92 Å) is smaller than that of Mn^{2+} (0.97 Å) [25].

Fig. 2 presents SEM images of the C–$LiMn_{1-x}Fe_xPO_4$ powders (x = 0 and 0.15). The images show that both powders were composed of agglomerated nanoparticles; however, C–$LiMn_{0.85}Fe_{0.15}PO_4$ has a rough surface texture compared to C–$LiMnPO_4$. The SEM image in Fig. 2 suggests that the iron doping has visibly altered the powder morphology of C–$LiMnPO_4$. To verify the morphological difference, TEM analysis was carried on the two samples.

A TEM image in Fig. 3(a) shows carbon particles uniformly distributed among primary $LiMnPO_4$ particles whose size ranged from 20 nm to 200 nm. A magnified image of C–$LiMnPO_4$ in Fig. 3(b) indicates the primary particles have well-defined polygonal shapes with smooth edges which agree with the SEM image in Fig. 2(a). Meanwhile, the C–$LiMn_{0.85}Fe_{0.15}PO_4$ powders had morphology clearly different from the undoped sample. As can be seen from Fig. 3(c), the primary particles have irregular shapes with relatively larger size compared to $LiMnPO_4$. Moreover, the primary particles are in intimate contact with the carbon particles such that the carbon particles formed an entangled network among the primary particles. A high-resolution TEM image of C–$LiMn_{0.85}Fe_{0.15}PO_4$ in

Table 1
Lattice parameters of C–$LiMn_{1-x}Fe_xPO_4$ (x = 0 and 0.15) powders.

	a (Å)	b (Å)	c (Å)	V (Å^3)
$LiMnPO_4$	10.4628	6.1054	4.7453	303.128
$LiMn_{0.85}Fe_{0.15}PO_4$	10.3787	6.0765	4.7125	297.199

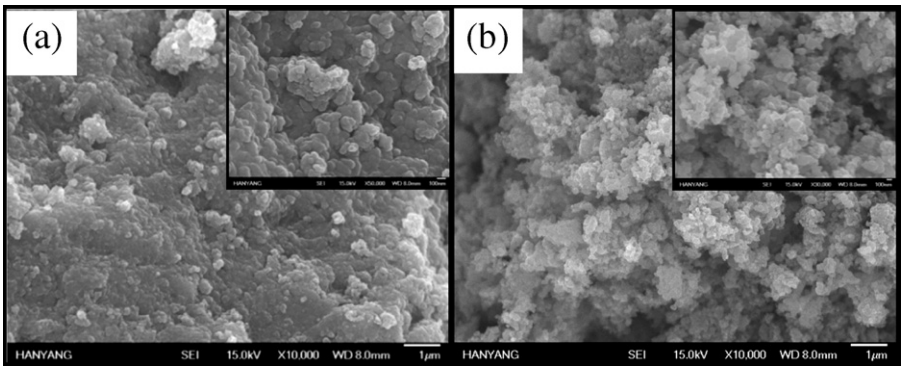

Fig. 2. SEM images of C–$LiMn_{1-x}Fe_xPO_4$ powders: (a) $x = 0$ and (b) $x = 0.15$.

Fig. 3(d) shows carbon lattice fringes growing on the surface of a C–$LiMn_{0.85}Fe_{0.15}PO_4$ particle which was not observed on the C–$LiMnPO_4$ powder. As iron is often employed as a catalyst for growing carbon nanotubes and other carbon-based nanostructures [26], it is plausible that the iron doping increased the chemical affinity of $LiMnPO_4$ for carbon so that some of the carbonaceous material was able to grow on the particle surface. Also, it can be conjectured that the iron likely has a higher chemical affinity for carbon as iron produces more stable carbides compared to manganese (inferred from the melting point of the respective carbides [27]). Comparing the TEM images in Fig. 3(a) and (c), C–$LiMn_{0.85}Fe_{0.15}PO_4$ appears to have carbon particles tightly surrounding the primary particles compared to the C–$LiMnPO_4$ powder, which should improve the electrical conductivity of the C–$LiMn_{0.85}Fe_{0.15}PO_4$ powders. In addition, the surface roughness of the C–$LiMn_{0.85}Fe_{0.15}PO_4$ primary particles should provide an increased pore volume when compacted, compared to C–$LiMnPO_4$ which is shown in Table 2. These morphological features should expedite the Li-ion transport through the Fe-doped electrode. The TEM analysis clearly identified the morphological change brought by the Fe doping, which should enhance the electrochemical properties of the C–$LiMn_{0.85}Fe_{0.15}PO_4$ electrode.

Fig. 4(a) presents the first charge–discharge curves of the Li/C–$LiMn_{1-x}Fe_xPO_4$ cells ($x = 0$ and 0.15). The cells were charged to 4.5 V in a constant current–constant voltage mode at a 1/20*C*-rate, held until 1/100*C*-rate, and discharged to 2.7 V at

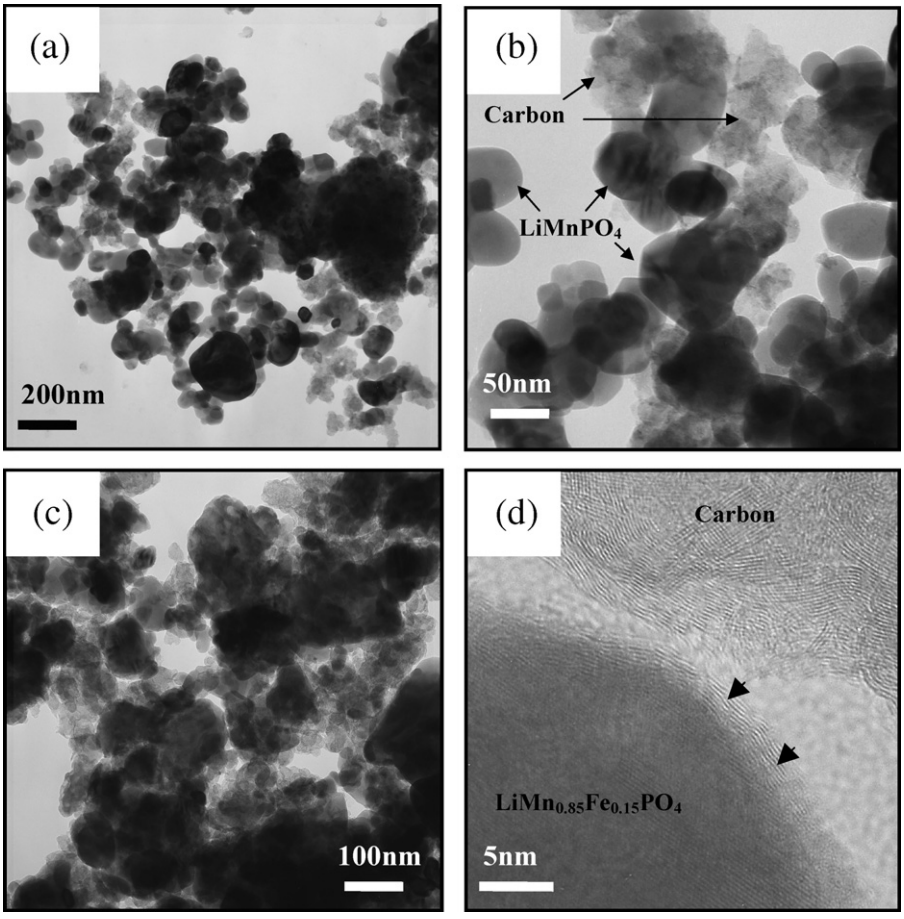

Fig. 3. TEM images of (a) C–$LiMnPO_4$ powder, (b) magnified image of (a), (c) C–$LiMn_{0.85}Fe_{0.15}PO_4$ powder, and (d) high-resolution image of $LiMn_{0.85}Fe_{0.15}PO_4$ powder with arrows indicating the surface-grown carbon material.

Table 2
Physical properties of C–$LiMn_{1-x}Fe_xPO_4$ (x = 0 and 0.15) powders.

	Conductivity ($S\,cm^{-1}$)	Pore volume ($cm^3\,g^{-1}$)	Mn dissolution (ppm)[a]
$LiMnPO_4$	4.3×10^{-1}	2.014×10^{-1}	103.7
$LiMn_{0.85}Fe_{0.15}PO_4$	7.4×10^{-1}	2.761×10^{-1}	87.2

[a] Mn dissolution for the electrolyte was carried out in the fully charged state of 4.5 V after 4 weeks at 55 °C (1 M $LiPF_6$ in EC:DEC = 1:1).

a constant current of 1/20*C*-rate (8.5 mAh g^{-1}) at 25 °C. The C–$LiMnPO_4$ electrode exhibited a reversible plateau around 4.1 V vs. Li/Li^+, corresponding to the redox couple of Mn^{3+}/Mn^{2+} whereas C–$LiMn_{0.85}Fe_{0.15}PO_4$ electrode shows two plateaus at 4.1 V and 3.5 V related to the Mn^{3+}/Mn^{2+} and the Fe^{2+}/Fe^{3+} redox couples. The C–$LiMn_{0.85}Fe_{0.15}PO_4$ electrode delivered a slightly higher discharge capacity of 163 mAh g^{-1} than C–$LiMnPO_4$ electrode (158 mAh g^{-1}). In order to exactly locate the redox voltages during the first cycle, the 1st charge and discharge curves were differentiated and the result is shown in Fig. 4(b). Li/C–$LiMnPO_4$ cell has one pair of peaks, corresponding to the charge/discharge reaction of the Mn^{2+}/Mn^{3+} (charge: 4.18 V; discharge: 4.03 V) redox couple with polarization potential of 0.15 V. On the other hand, Li/C–$LiMn_{0.85}Fe_{0.15}PO_4$ cell has two pairs of peaks, related to the charge/discharge reaction of the Fe^{2+}/Fe^{3+} (charge: 3.57 V; discharge: 3.53 V) and Mn^{2+}/Mn^{3+} (charge: 4.13 V; discharge: 4.07 V) redox couples with polarization potential of 0.06 V for the Mn plateau. The reduced polarization potential for the Mn^{2+}/Mn^{3+} redox couple of the Li/C–$LiMn_{0.85}Fe_{0.15}PO_4$ cell suggests that the Mn^{2+}/Mn^{3+} redox resistance was decreased by the Fe doping. To verify the result,

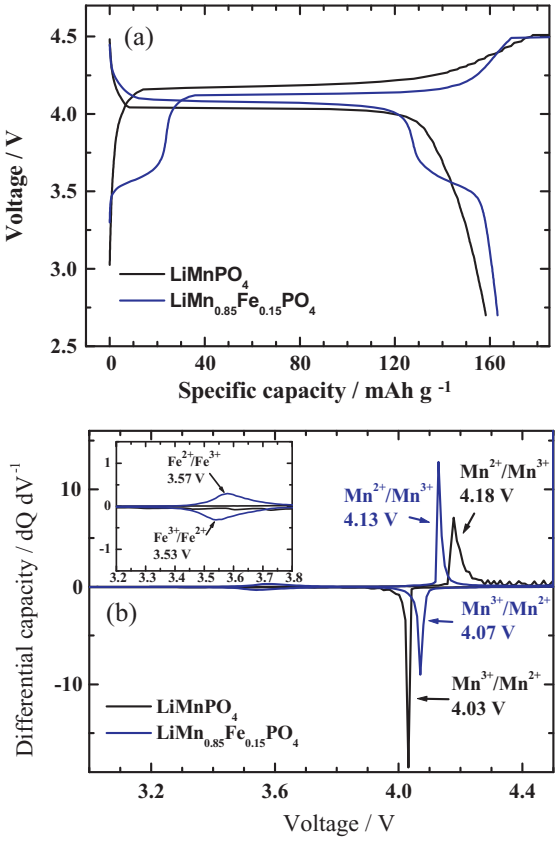

Fig. 4. (a) 1st charge/discharge curves of Li/C–$LiMn_{1-x}Fe_xPO_4$ (x = 0 and 0.15) cells charged with at a constant current/20*C*-rate to 4.5 V, held at 4.5 V until 1/100*C*-rate, and discharged with at a constant current 1/20*C*-rate to 2.7 V and (b) corresponding d*Q*/d*V* curves.

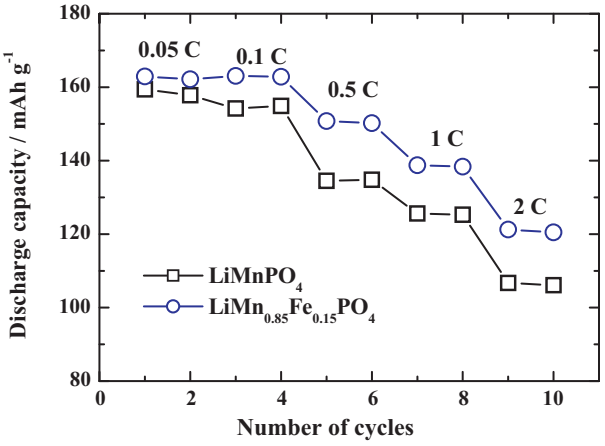

Fig. 5. Rate capability of Li/C–$LiMn_{1-x}Fe_xPO_4$ (x = 0 and 0.15) cells between 2.7 V and 4.5 V. The cell was charged with a constant current of 1/20*C*-rate to 4.5 V and kept at 4.5 V until 1/100*C*-rate.

electronic conductivity of the electrodes with a four-point probe and pore volume with N_2 adsorption were measured. The results are summarized in Table 2. As conjectured from the TEM analysis, the electronic conductivity of C–$LiMn_{0.85}Fe_{0.15}PO_4$ powders nearly doubled by the Fe doping. In the case of the pore volume, the pore volume of C–$LiMn_{0.85}Fe_{0.15}PO_4$ was also larger than that of C–$LiMnPO_4$. The large pore volume should be beneficial for C–$LiMn_{0.85}Fe_{0.15}PO_4$ as the increased pore volume contributes to penetration of electrolytes which increase the electrochemical properties of C–$LiMn_{0.85}Fe_{0.15}PO_4$ [28]. The morphological superiority and carbon coating layer on surface of C–$LiMn_{0.85}Fe_{0.15}PO_4$ particles observed in the TEM analysis was clearly manifested in the electronic conductivity and pore volume measurements which resulted in the overall improvement of the C–$LiMn_{0.85}Fe_{0.15}PO_4$ electrode.

Rate capability for the Li/C–$LiMn_{1-x}Fe_xPO_4$ (x = 0 and 0.15) cells is shown in Fig. 5. The cells were discharged at an increasingly higher current starting from 1/20 to 10*C*-rate at 25 °C. Before discharge, each cell was charged with a constant current of 1/20*C*-rate to 4.5 V and kept at 4.5 V until 1/100*C*-rate. As expected, the C–$LiMn_{0.85}Fe_{0.15}PO_4$ electrode showed better rate capability than the C–$LiMnPO_4$ electrode. For example, the C–$LiMn_{0.85}Fe_{0.15}PO_4$ delivered a discharge capacity of 121 mAh g^{-1} at 2*C*-rate, showing the capacity retention of 74% compared with that of 0.05*C*-rate, whereas the C–$LiMnPO_4$ reached 107 mAh g^{-1} having capacity retention of 67%. The improved rate capability of the C–$LiMn_{0.85}Fe_{0.15}PO_4$ is likely due to the higher electrical conductivity and larger pore volume of the C–$LiMn_{0.85}Fe_{0.15}PO_4$ as demonstrated in Table 2.

Fig. 6 shows discharge capacity of Li/C–$LiMn_{1-x}Fe_xPO_4$ (x = 0 and 0.15) cells over 50 cycles at 25 °C and 55 °C. Testing was done at 0.5*C*-rate between 2.7 V and 4.5 V. The two electrodes showed very stable cycling performance of 94% after 50 cycles at 25 °C though the C-$LiMn_{0.85}Fe_{0.15}PO_4$ had a higher discharge capacity (151 mAh g^{-1}) than C–$LiMnPO_4$ (137 mAh g^{-1}). However, the capacity retention of C–$LiMnPO_4$ at 55 °C dropped to 87% at the same cycling period while the C–$LiMn_{0.85}Fe_{0.15}PO_4$ exhibited enhanced capacity retention of 91%. Similar to previous results with spinel $LiMn_2O_4$ [29], we speculate that Mn dissolution into electrolyte is directly related to capacity fade shown in Fig. 6(b). Thus, the concentration of dissolved Mn in the ethylene carbonate (EC)/diethyl carbonate (DEC) electrolyte was measured by AAS and the result was shown in Table 2. It was observed that a smaller amount of Mn was dissolved for the C–$LiMn_{0.85}Fe_{0.15}PO_4$. The dissolved amount of Mn for the C–$LiMnPO_4$ was approximately 104 ppm while the

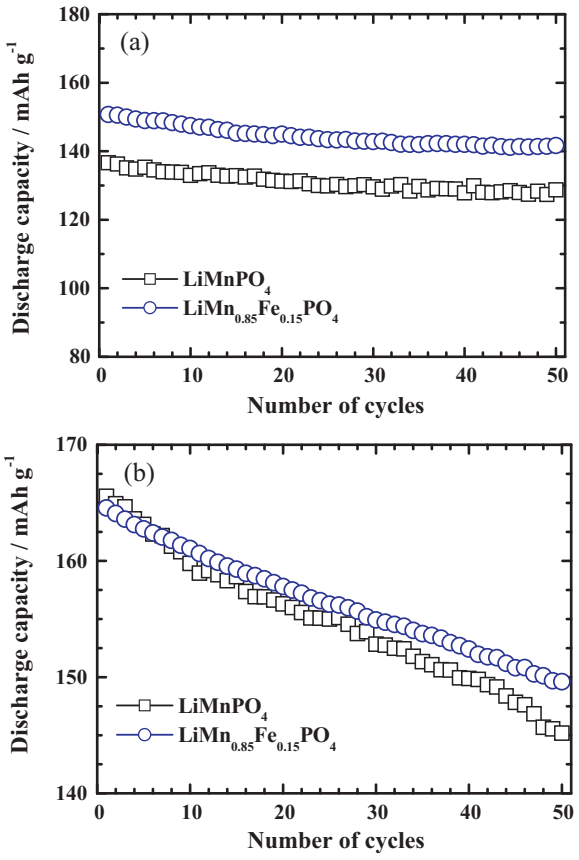

Fig. 6. Discharge capacity versus number of cycle for Li/C–$LiMn_{1-x}Fe_xPO_4$ (x = 0 and 0.15) cells at 0.5*C*-rate (a) cycled at 25 °C and (b) cycled at 55 °C. The cell was charged with a constant current of 1/20*C*-rate to 4.5 V and kept at 4.5 V until 1/100*C*-rate.

C–$LiMn_{0.85}Fe_{0.15}PO_4$ exhibited reduced Mn dissolution in the electrolyte, having a concentration of about 87 ppm. The Mn dissolution test result is well in accordance with TEM result and electrochemical performance. Hence, we believe that the uniform carbon coating on the C–$LiMn_{0.85}Fe_{0.15}PO_4$ protects the particle surface from HF attack and thus reduced Mn dissolution, which improved the electrochemical performance.

4. Conclusions

Nano-structured C–$LiMn_{1-x}Fe_xPO_4$ (x = 0 and 0.15) nanocomposite were synthesized by ultrasonic pyrolysis followed by ball milling with carbon, and the electrochemical performance was studied. Analysis by SEM and TEM exhibited the homogeneous dispersion of AB carbon coating over the $LiMn_{0.85}Fe_{0.15}PO_4$ particle. The C–$LiMn_{0.85}Fe_{0.15}PO_4$ delivered a discharge capacity of 121 mAh g^{-1} at 2*C*-rate, whereas the C–$LiMnPO_4$ reached only 107 mAh g^{-1}. The capacity retention of the C–$LiMn_{0.85}Fe_{0.15}PO_4$ after 50 cycles at 55 °C was 91% while that of the C–$LiMnPO_4$ was 87% compared with the initial discharge capacity. These improved electrochemical properties were ascribed to the coating effect of AB carbon which was thought to exert its positive effect by improving electronic conductivity and suppressing Mn dissolution from the C–$LiMn_{0.85}Fe_{0.15}PO_4$.

Acknowledgements

This research was supported by a National Research Foundation of Korea (NRF) grant funded by the Korean government (MEST) (No. 2009-0092780) and grant funded from the Ministry of Education, Science and Technology (MEST) of Korea for the Center for Next Generation Dye-sensitized Solar Cells (No.2009-0063371).

References

[1] A.K. Padhi, K.S. Nanjundaswamy, J.B. Goodenough, J. Electrochem. Soc. 144 (1997) 1188.
[2] S.-Y. Chung, J.T. Bloking, Y.-M. Ching, Nat. Mater. 1 (2002) 123.
[3] A.S. Andersson, J.O. Thomas, B. Kalsa, L. Haggstroem, Electrochem. Solid-State Lett. 3 (2000) 66.
[4] A. Yamada, S.C. Chung, K. Hinokuna, J. Electrochem. Soc. 148 (2001) A224.
[5] M.M. Doeff, Y. Hu, F. McLarnon, R. Kostecki, Electrochem. Solid-State Lett. 6 (2003) A207.
[6] D. Zane, M. Carewska, S. Scaccia, F. Cardellini, P.P. Prosini, Electrochim. Acta 49 (2004) 4259.
[7] K. Dokko, S. Koizumi, K. Sharaishi, K. Kanamura, J. Power Sources 165 (2006) 656.
[8] N. Ravet, S. Besner, M. Simoneau, A. Valleĭe, M. Armand, Hydro-Queĭbec, Can. Pat. 2,270,771.
[9] H. Huang, S.C. Yin, L.F. Nazar, Electrochem. Solid-State Lett. 4 (2001) A170.
[10] M. Yonemura, A. Yamada, Y. Takei, N. Sonoyama, R. Kanno, J. Electrochem. Soc. 151 (2004) A1352.
[11] G. Li, H. Azuma, M. Tohda, Electrochem. Solid-State Lett. 5 (2002) A135.
[12] N.-H. Kwon, T. Drezen, I. Exnar, I. Teerlinck, M. Isono, M. Graetzel, Electrochem. Solid-State Lett. 9 (2006) A277.
[13] C. Delacourt, P. Poizot, M. Morcrette, J.M. Tarascon, C. Masquelier, Chem. Mater. 16 (2004) 93.
[14] T. Drezen, N.-H. Kwon, P. Bowen, I. Teerlinck, M. Isono, I. Exnar, J. Power Sources 174 (2007) 949.
[15] J. Xiao, W. Xu, D. Choi, J.-G. Zhang, J. Electrochem. Soc. 157 (2010) A142.
[16] S.K. Martha, B. Markovsky, J. Grinblat, Y. Gofer, O. Haik, E. Zinigrad, D. Aurbach, T. Drezen, D. Wang, G. Deghenghi, I. Exnar, J. Electrochem. Soc. 156 (2009) A541.
[17] D. Wang, H. Buqa, M. Crouzet, G. Deghenghi, T. Drezen, I. Exnar, N.-H. Kwon, J.H. Miners, L. Poletto, M. Grätzel, J. Power Sources. 189 (2009) 624.
[18] Z. Bakenov, I. Taniguchi, Electrochem. Commun. 12 (2010) 75.
[19] S.-M. Oh, S.-W. Oh, C.-S. Yoon, B. Scrosati, K. Amine, Y.-K. Sun, Adv. Func. Mater 20 (2010) 3260.
[20] T. Shiratsuchi, S. Okada, T. Doi, J. Yamaki, Electrochim. Acta 54 (2009) 3145.
[21] D. Wang, C. Ouyang, T. Drezen, I. Exnar, A. Kay, N.-H. Kwon, P. Gouerec, J. Miners, M. Wang, M. Gratzel, J. Electrochem. Soc. 157 (2010) A225.
[22] A. Yamada, S.-C. Chung, J. Electrochem. Soc. 148 (2001) A960.
[23] S.K. Martha, J. Grinblat, O. Haik, E. Zinigrad, T. Drezen, J.H. Miners, I. Exnar, A. Kay, B. Markovsky, D. Aurbach, Angew. Chem. Int. Ed. 48 (2009) 1.
[24] J. Molenda, W. Ojczyk, J. Marzec, J. Power Sources. 174 (2007) 689.
[25] R.D. Shannon, Acta Crystallogr. A32 (1976) 751.
[26] B. Ha, T.H. Yeom, S.H. Lee, Physica B 404 (2009) 1617.
[27] S.T. Oyama, The Chemistry of Transition Metal Carbides and Nitrides, Blackie Academic & Professional, Glasgow, 1996, pp. 1–27.
[28] R. Dominko, J.M. Goupil, M. Bele, M. Gaberscek, M. Remskar, D. Hanzel, J. Jamnik, J. Electrochem. Soc. 152 (2005) A858.
[29] Y. Xia, Y. Zhou, M. Yoshio, J. Electrochem. Soc. 144 (1997) 2593.